

Functional Renormalisation Group for Brownian Motion I: Equilibrium

Ashley Wilkins* and Gerasimos Rigopoulos†
School of Mathematics, Statistics and Physics, Newcastle University,
Newcastle upon Tyne, NE1 7RU, United Kingdom

Enrico Masoero‡
School of Engineering, Newcastle University,
Newcastle upon Tyne, NE1 7RU, United Kingdom
(Dated: June 8, 2022)

We use the functional Renormalisation Group (fRG) to describe the equilibrium state of stochastic processes governed by an overdamped Langevin equation in highly anharmonic potentials. Exploiting the connection between Langevin dynamics and supersymmetric quantum mechanics in imaginary time, we obtain renormalisation flow equations for the effective action, approximated in terms of the Local Potential Approximation and Wavefunction Renormalisation which we solve numerically. The obtained effective potential determines exactly the equilibrium position $\langle x \rangle$, the variance $\langle (x - \langle x \rangle)^2 \rangle$, as well as all higher order cumulants. The equilibrium 2-point correlation function $\langle x(0)x(t) \rangle$ and the relevant correlation time can also be obtained to percent accuracy when Wavefunction Renormalisation is utilized. The numerical computations determining the effective action are much faster than the direct simulation of the stochastic dynamics to which we compare our fRG results. A companion paper will examine the application of the fRG to this system when the initial state is not that of equilibrium.

I. INTRODUCTION

Stochastic processes appear in all kinds of contexts in physics. From the Brownian motion of small particles in a thermal bath [1, 2] to scalar fields experiencing quantum fluctuations in the early inflationary universe [3], many problems of interest can be described by the overdamped Langevin equation (4). However, the fluctuations (thermal or effectively thermal) occur very frequently and if one were to attempt to adequately simulate such a process a suitable small timestep size would have to be chosen. This means we only have an immediate understanding of the physics on small timescales. Understanding long-time behaviour and finding the equilibrium properties of the system from its initial out-of-equilibrium state requires following the stochastic process for times much longer than this fundamental timescale. It is natural therefore to ask if a ‘coarse grained’ description in time would be beneficial in tracking the long time behaviour at reduced computational cost. This desire to coarse-grain time and examine physics on different temporal scales lends itself naturally to the tools of the Renormalisation Group (RG).

The renormalisation group was brought to full force through the work of K. Wilson [4] who used it to understand phase transitions and since then the RG has become a widely used technique in modern physics with many applications in both particle physics [5] and condensed matter physics [6]. The RG is relevant whenever

fluctuations significantly influence the state (static or dynamical) of a physical system. Its conceptual framework as applied in condensed matter is perhaps most apt for describing the goal in this work: the RG interpolates between a small lattice size, where the underlying physics is known, to a much larger lattice size by including the effect of fluctuations on all intermediate length scales, providing an *effective* picture that averages over all such fluctuations. In this work we apply this idea to the stochastic dynamics of a Brownian particle. For us the small lattice size corresponds to a small fundamental timescale over which the dynamics is adequately described by the Langevin equation (4). We seek an effective description, valid over much longer timescales, that captures the aggregate effect of fluctuations. The effective description is embodied in an *effective action* $\Gamma[\chi(t)]$ of the average position $\chi(t) \equiv \langle x(t) \rangle$. In particular, one can use the effective action to compute n -point correlation functions of the particle’s position $\langle x(t_1)x(t_2) \dots x(t_n) \rangle$, characterizing the system’s statistical properties. To obtain this effective long-time behaviour we will use a version of the RG known as the functional or exact or non-perturbative Renormalisation Group.

The functional Renormalisation Group (fRG) offers advantages compared to other formulations of the RG, including its ability to deal with theories with strong couplings and its focus on a single object, the effective action Γ . These features will allow us to study stochastic motion in non-harmonic potentials with arbitrary shapes that do not offer themselves to be studied straightforwardly via standard perturbative RG methods more commonly employed. The effective action can be thought of as an analogue to the statistical free energy and can be derived from the partition function or generating functional via

* a.wilkins3@newcastle.ac.uk

† gerasimos.rigopoulos@newcastle.ac.uk

‡ enrico.masoero@newcastle.ac.uk

a Legendre transform. Wetterich showed [7] - see also [8] - how one can define Γ at some particular energy or momentum scale Λ in the UV (small timestep/high frequency for us) where the theory is known and then create an RG flow that interpolates between all energy scales down to the IR (i.e. increasing timestep size/decreasing frequency). This changing of the effective theory at different energy scales or lattice sizes, the fundamental idea behind the RG, can be formulated in a differential equation known as the Wetterich equation:

$$k\partial_k\Gamma_k = \frac{1}{2}\mathbf{Tr}\left[k\partial_k R_k\left(\Gamma_k^{(2)} + R_k\right)^{-1}\right] \quad (1)$$

where Γ_k is the effective action at energy scale (frequency/momentum) k , \mathbf{Tr} denotes a trace over spatio-temporal points (an integral over spacetime) and a trace over all other relevant indices, R_k is an IR regulator that acts as a cut-off for fluctuations below energy scale/frequency k , and $\Gamma_k^{(2)}$ is the second functional derivative of Γ_k - see [9] for a review and an entry point to the literature on the subject as well as e.g. [10, 11] for more elementary introductions. See also appendix C for a simple manifestation of this flow equation for equilibrium.

In this work we put equation (1) to use for studying the dynamics of particles under the influence of a deterministic force, stemming from an arbitrary potential, and thermal fluctuations. We start in Sec. II by reviewing the connection between Langevin dynamics and SuperSymmetric quantum mechanics in imaginary time first shown in [12] - for another review see e.g. [13]. The corresponding path integral formulation then allows us to apply the fRG program directly. Although the fRG has been applied to Langevin dynamics before [14], as far as the authors are aware the underlying SuperSymmetry has only been very recently utilized in the context of stochastic inflationary dynamics [15–17]. Exploiting the underlying Supersymmetry simplifies the computation of the Wetterich equation (1) which was first derived in this setup in [18]. In fact, it can be shown that the physically inspired conditions the authors of [14] require of their flow equations are straightforwardly imposed by requiring that the Supersymmetry remains unbroken during the flow [16].

In Sec. III we present the flow equations for the effective action utilising the results of [18] for supersymmetric RG flows. To turn the functional integro-differential equation (1) into a mathematically more tractable form we employ two commonly used approximations for the effective action Γ_k : the Local Potential Approximation (LPA) as well as the LPA augmented by Wavefunction Renormalisation. As we discuss, the LPA offers a clear physical interpretation for the effective action: as the effect of fluctuations is progressively taken into account during the flow, the effective potential $V_k(x)$ experienced by the particle is altered, compared to the bare, fundamental potential $V(x)$. Wavefunction Renormalisation (WFR) involves a second function $Z_k(x)$ which can be

interpreted as a redefinition of position $x \rightarrow Z(x)$.

In Sec. IV we discuss how the fRG can give us observable quantities that could be measured in simulations. These are in the form of n -point connected correlation functions, or Ursell functions, which can be obtained from $\Gamma_{k=0}$ in a standard way. In particular, we demonstrate how the effective potential and wave function renormalization provide the average position, variance and the time dependence of the connected 2-point function, while also discussing how higher order correlation functions like the 3-point and 4-point functions can in principle be obtained for particles in equilibrium.

Sec. V contains our main results. We present numerical solutions to the flow equations for three types of anharmonic bare potentials: a polynomial asymmetric potential, a symmetric quartic double well and an asymmetric, double Lennard-Jones. We consider two temperatures, a relatively high one and a low one, controlling the amplitude of fluctuations and, naturally, the end result of the flow equations. Using the obtained effective potentials $V_{k\rightarrow 0}$ we evaluate the mean position of the particle $\langle x \rangle$ and its variance $\langle x^2 \rangle - \langle x \rangle^2$ at equilibrium and find excellent agreement with the exact results from the equilibrium Boltzmann distribution. This provides confirmation that the numerical solution of the LPA flow equation is accurate.

We also examine the characteristic decay behaviour of the 2-point function $\langle x(0)x(t) \rangle$ at equilibrium by utilizing both the effective potential $V_{k\rightarrow 0}$ and the WFR function $Z_{k\rightarrow 0}$. We evaluate how these fRG predictions compare to results from numerical simulations of the random walk and find very good agreement between them and the simulations at both high and low temperatures. Where possible we also compare with the characteristic decay time obtained by exactly solving the corresponding Schroedinger equation (derived from the Fokker-Planck equation) for the lowest eigenvalue. We find that the the LPA + WFR fRG equations give a comparable match to the true decay rate at the percent level.

We conclude in Sec. VI by summarising our main results. In Appendix A we show that our results also apply for two mutually interacting particles in 2D and 3D, Appendix B recalls the relation of the Langevin dynamics to an imaginary time Schrödinger equation via the more familiar route of the Fokker-Planck equation while Appendix C derives the analogue of the Wetterich equation (1) for the effective potential corresponding to the equilibrium Boltzmann distribution. The present paper deals with particles that have reached equilibrium. A forthcoming, companion paper will apply the fRG to the dynamical evolution of averaged quantities from generic, non-equilibrium initial conditions as well as escape problems.

II. BROWNIAN MOTION AS SUPERSYMMETRIC QUANTUM MECHANICS

Brownian motion for a single particle of mass m moving in a potential $V(x)$, coupled to an external heat bath with temperature T , can be described by the Langevin equation:

$$m\ddot{x} + \gamma\dot{x} = -\partial_x V(x) + f(t) \quad (2)$$

$$\langle f(t)f(t') \rangle = 2D\gamma^2\delta(t-t') \quad (3)$$

where γ is a frictional term due to the surrounding fluid and $f(t)$ is a gaussian ‘‘noise’’ term. $D = k_b T/\gamma$ is the diffusion constant with equality given so as to match the Boltzmann equilibrium distribution (should it exist). Hereafter, we will be concerned with the overdamped limit which corresponds to $\varepsilon \equiv m/\gamma$ being a short timescale compared to the time scales of interest:

$$\dot{x} = -\varepsilon\partial_x \bar{V}(x) + \eta(t) \quad (4)$$

$$\langle \eta(t)\eta(t') \rangle = 2D\delta(t-t') \quad (5)$$

Here we have taken out a mass factor from the potential V so that mass appears explicitly in the equation (i.e. $V = m\bar{V}$). For convenience we will drop the overbar from here on in. This movement of a single particle in 1-D can also be used to describe the radial separation of two particles moving in 2-D or 3-D – see Appendix A.

The treatment we cover in this paper will be applicable to any potential described by a continuous & differentiable function on the domain of interest¹. The potentials we will use as a case study are a simple polynomial:

$$V(x) = x + \frac{x^2}{2} + \frac{gx^3}{3} + \frac{x^4}{4} \quad (6)$$

with $g > 0$; the doublewell:

$$V(x) = ax^2 + bx^4 \quad (7)$$

with $a < 0$ and $b > 0$; and a doublewell made by two Lennard-Jones (LJ) potentials back to back:

$$V(x) = 4\epsilon_1 \left(\frac{\sigma^{12}}{(x+3)^{12}} - \frac{\sigma^6}{(x+3)^6} \right) + 4\epsilon_2 \left(\frac{\sigma^{12}}{(x-3)^{12}} - \frac{\sigma^6}{(x-3)^6} \right) \quad (8)$$

where σ will be taken to be 1 from here on in and ϵ_1 & ϵ_2 represents the depth of each well. E.g. if $\epsilon_1 = \epsilon_2 = 1$ both wells are 1 unit deep and the potential is symmetric. Clearly here the domain of interest is $x \in (-3, 3)$ as the potential diverges at $x = \pm 3$. Unless otherwise stated our chosen parameters will be:

$$\text{Doublewell: } a = -1, b = 1/4 \quad (9)$$

$$\text{Poly: } g = 2 \quad (10)$$

$$\text{Unequal L-J: } \epsilon_1 = 1, \epsilon_2 = 10, \sigma = 1 \quad (11)$$

¹ In actuality the only strict condition is that $V(x)$ is twice/thrice differentiable for LPA/WFR i.e. $V(x) \in C^2(x)$ for LPA & $V \in C^3(x)$ for WFR

A. The Brownian Motion Path Integral

In order to bring the powerful tools of Quantum Field Theory such as the fRG to bear, we will need to reformulate the stochastic differential equation (4) in terms of a *path integral*. In this subsection we will outline one way to obtain this path integral, aiming to link this to Supersymmetric Quantum Mechanics. Our final expression, and the starting point of our subsequent analysis, is the Brownian Motion transition probability (22), expressed in terms of an integral over possible histories weighted by the action (23), to which the busy reader may progress if uninterested in the details of the derivation. We will be using a condensed functional notation of infinite dimensional functional integrals but all expressions can be considered as limits of large, finite dimensional ordinary integrals. More details on these path integrals, including the corresponding finite discretisation of the stochastic process can be found in [19].

The dynamics of the Langevin equation (4) can be captured in terms of the *Probability Distribution Function* (PDF) $\mathcal{P}(x_f|x_i)$ of observing the particle at x_f at time $t = t_f$ given that initially at $t = t_i$ the particle was at x_i . By definition this can be expressed as:

$$\mathcal{P}(x_f|x_i) = \langle \delta(x(t_f) - x_f) \rangle \quad (12)$$

where the expectation value is taken over all possible realisations of the noise $\eta(t)$ and $\delta(x(t_f) - x_f)$ is the Dirac delta function. Put another way, $x(t_f)$ is the position at t_f for a given noise history $\eta(t)$ and the brackets indicate averaging over all possible noise histories, or stochastic paths, which start at x_i and end up at $x(t_f) = x_f$ at t_f . This is precisely a path integral so we can rewrite the PDF using a gaussian measure for noise (5) and express the average as

$$\mathcal{P}(x_f|x_i) = \int \mathcal{D}\eta(t) \delta(x(t_f) - x_f) \exp \left[- \int dt \frac{\eta^2}{4D} \right] \quad (13)$$

where each noise history is weighted by the exponential factor in the above expression. We now consider the identity (see e.g. [13]):

$$1 = \int dx_f \int_{x_i}^{x_f} \mathcal{D}x(t) \delta(x(t) - x_\xi(t)) \quad (14)$$

$$= \int dx_f \int_{x_i}^{x_f} \mathcal{D}x(t) \delta(\dot{x} + \varepsilon V_{,x} - \eta(t)) \det \mathbf{M} \\ = \int_{x_i} \mathcal{D}x(t) \delta(\dot{x} + \varepsilon V_{,x} - \eta(t)) \det \mathbf{M} \quad (15)$$

where the matrix \mathbf{M} is:

$$\mathbf{M} \equiv \frac{\delta\eta}{\delta x} = \frac{d}{dt} + \varepsilon V_{,xx} \quad (16)$$

expressing the obvious fact that, if the particle starts at some x_i and follows a particular history $x_\xi(t)$ dictated by the Langevin equation without disappearing, it will end

up somewhere after time t_f . We have used the standard subscript notation to denote derivative with respect to that variable e.g. $V_{,xx} = \partial_{xx}V$. Note that the second path integral in (15) is over all paths starting at x_i at t_i and ending at any x at t_f . Inserting our ‘fat unity’ factor (15) into (13) and noting that our original delta function restricts $x(t_f)$ to be x_f we obtain:

$$\mathcal{P}(x_f|x_i) = \int_{x(t_i)=x_i}^{x(t_f)=x_f} \mathcal{D}\eta \mathcal{D}x \delta(\dot{x} + \varepsilon V_{,x} - \eta) \det \mathbf{M} \times \exp \left[- \int dt \frac{\eta^2}{4D} \right] \quad (17)$$

where the $\mathcal{D}x(t)$ integral is taken over all paths beginning at x_i and ending at x_f . We can rewrite the delta function as a functional Fourier transform using a new variable \tilde{x} which is usually called the *response field*:

$$\delta(\dot{x} + \varepsilon V_{,x} - \eta) = \int \mathcal{D}\tilde{x} \exp \left[i \int dt \tilde{x} (\dot{x} + \varepsilon V_{,x} - \eta) \right] \quad (18)$$

There are a couple of standard ways we can incorporate $\det \mathbf{M}$ into an exponential. A common way is using linear algebra and the Stratonovich description ($\theta(0) = 1/2$):

$$\det \mathbf{M} = \exp [\text{Tr} \log (\mathbf{M})] = \exp \left[\frac{\varepsilon}{2} \int dt V_{,xx} \right] \quad (19)$$

However to make clearer the link with SUSY we will instead using anticommuting variables² c and \bar{c} such that:

$$\det \mathbf{M} = \int \mathcal{D}\bar{c} \mathcal{D}c \exp \left[\int dt \bar{c} (\partial_t + \varepsilon V_{,xx}) c \right] \quad (20)$$

Inserting equations (18) & (20) into (17) we obtain:

$$\mathcal{P}(x_f|x_i) = \int \mathcal{D}\eta \mathcal{D}x \mathcal{D}\tilde{x} \mathcal{D}\bar{c} \mathcal{D}c \exp \left[\int dt - \frac{\eta^2}{4D} + i\tilde{x} (\dot{x} + \varepsilon V_{,x} - \eta) + \bar{c} (\partial_t + \varepsilon V_{,xx}) c \right] \quad (21)$$

We can now trivially perform the gaussian integral over η to obtain the path integral in terms of the Brownian Motion (BM) action $\mathcal{S}_{BM}(x, \tilde{x}, \bar{c}, c)$:

$$\mathcal{P}(x_f|x_i) = \int \mathcal{D}x \mathcal{D}\tilde{x} \mathcal{D}\bar{c} \mathcal{D}c \exp [-\mathcal{S}_{BM}(x, \tilde{x}, \bar{c}, c)] \quad (22)$$

$$\mathcal{S}_{BM}(x, \tilde{x}, \bar{c}, c) = \int dt \left[D\tilde{x}^2 - i\tilde{x}(\dot{x} + \varepsilon V_{,x}) - \bar{c}(\partial_t + \varepsilon V_{,xx})c \right] \quad (23)$$

Computing this path integral which henceforth shall be called the *Brownian Path Integral* (BPI) is in general impossible analytically. Instead we will be using the fRG to compute it numerically using the appropriate flow equation. Redefining our fields as :

$$\begin{aligned} x(t) &\equiv \sqrt{2D}\varphi(t) \\ V(x) &\equiv \frac{2D}{\varepsilon}W(\varphi) \\ \tilde{x} &\equiv \frac{1}{\sqrt{2D}}(i\dot{\varphi} - F) \\ \bar{c}c &\equiv i\bar{\psi}\psi \end{aligned} \quad (24)$$

we obtain

$$\mathcal{S}_{BM}[\varphi, F, \bar{\psi}, \psi] = [W(\varphi_f) - W(\varphi_i)] + \mathcal{S}_{SUSY} \quad (25)$$

where

$$\mathcal{S}_{SUSY}[\varphi, F, \bar{\psi}, \psi] = \int dt \left[\frac{1}{2} \dot{\varphi}^2 + \frac{1}{2} F^2 + iFW_{,\varphi}(\varphi) - i\bar{\psi}(\partial_t + W_{,\varphi\varphi}(\varphi))\psi \right] \quad (26)$$

Action (26) describes the dynamics of Euclidean, or imaginary time, Supersymmetric Quantum Mechanics where ψ & $\bar{\psi}$ are the fermionic fields and φ & F are the bosonic fields. We have shown that the same action also describes Brownian motion and the BM action is equivalent to the SUSY QM one up to a factor depending on the initial and final positions x_i & x_f . As the integrand of the BPI (22) does not depend on the final or initial states this (now exponential) factor simply comes outside the integral as a constant that can be absorbed when the PDF is normalised. Variation of \mathcal{S}_{SUSY} w.r.t. F yields its ‘equation of motion’ $F = -iW_{,\varphi}$ which when substituted back into \mathcal{S}_{SUSY} yields the ‘on mass-shell’ action

$$\mathcal{S}_{OM}[\varphi, \bar{\psi}, \psi] = \int dt \left[\frac{1}{2} \dot{\varphi}^2 + \frac{1}{2} W_{,\varphi}^2 - i\bar{\psi}(\partial_t + W_{,\varphi\varphi})\psi \right] \quad (27)$$

The fRG was first applied to a system governed by (26) by Synatschke et. al [18] whose approach we adopt in what follows - see also [20].

III. APPLYING THE FUNCTIONAL RENORMALISATION GROUP

The formulation of the fRG involves a functional (infinite dimensional) differential equation known as the Wetterich equation [7] that describes the ‘flow’ of the effective action between the microscopic and macroscopic scale. This ‘flow’ is described by a parameter k that ranges from the UV cutoff Λ down to the IR regime as $k \rightarrow 0$. In our Brownian motion scenario, microscopic regime refers to a

² These suggestively already look like fermionic fields which we will see they are related to in the Supersymmetric picture

small timestep and macroscopic to a long timestep. The definition of $\Lambda \sim 1/\Delta t$ is analogous to the Condensed Matter interpretation of the cutoff being inversely proportional to the lattice size, the only difference here being that the Condensed Matter lattice is in space and ours is in time. We will use the fRG ultimately to calculate correlation functions of the particle position at late times. Our basic equations are (43) for the Local Potential Approximation to the RG flow whereas when we also include Wavefunction Renormalisation they are (48) and (49). But first, we briefly recall how to generate correlation functions in the standard Field Theory way.

In Euclidean Quantum Field Theory correlation functions can be evaluated with the help of *generating functionals*. The most straightforward of these is the partition functional $\mathcal{Z}(J)$ which depends on a source term $J(x)$ (in analogy with a magnetic field source term $M(x)$ in spin systems). For concreteness the two point correlation function is:

$$\langle x(t_1)x(t_2) \rangle = \frac{1}{\mathcal{Z}(0)} \frac{\delta^2 \mathcal{Z}(J)}{\delta J(t_2) \delta J(t_1)} \Big|_{J=0} \quad (28)$$

$$\mathcal{Z}(J) = \int \mathcal{D}x \exp \left[-\mathcal{S}[x] + \int_t Jx \right] \quad (29)$$

where $\mathcal{S}[x]$ is the action and $\int_t = \int dt$. We have assumed in the above that \mathcal{S} depends only on a single variable $x(t)$ for notational brevity but the above formulae are modified straightforwardly for any number of variables $x_i(t)$ which can be coupled to corresponding sources $J_i(t)$. For example $x_i(t) \equiv (x(t), \tilde{x}(t), \bar{c}(t), c(t))$ in (22).

We can store the information encoded in $\mathcal{Z}(J)$ better in the object $\mathcal{W}[J]$:

$$\mathcal{W}[J] \equiv \ln(\mathcal{Z}(J)) \quad (30)$$

Which is the generator of connected correlation functions (or Ursell functions):

$$\langle x(t_1) \dots x(t_n) \rangle_C = \frac{\delta^n \mathcal{W}[J]}{\delta J(t_1) \dots \delta J(t_n)} \quad (31)$$

So for instance the connected 2 point function $G(t_1, t_2)$ is:

$$\begin{aligned} G(t_1, t_2) &\equiv \langle x(t_1)x(t_2) \rangle_C = \langle x(t_1)x(t_2) \rangle - \langle x(t_1) \rangle \langle x(t_2) \rangle \\ &= \frac{\delta^2 \mathcal{W}[J]}{\delta J(t_1) \delta J(t_2)} \end{aligned} \quad (32)$$

Computing $\mathcal{W}[J]$ directly however is very difficult. Standard approaches involve perturbative expansions leading to the well known diagrammatic Feynman rules. In this work we will calculate a related object, the *effective action* $\Gamma[\chi]$ given by the Legendre transform of $\mathcal{W}[J]$

$$\Gamma[\chi] = \int_t J\chi - \mathcal{W}[J] \quad (33)$$

where the field χ corresponds to the expectation value of x in the presence of the source field J , satisfying

$$\chi = \frac{\delta \mathcal{W}[J]}{\delta J} = \langle x \rangle_J \quad (34)$$

The fRG formulation adds a regulating term to the action in our definition of the generating functional:

$$\mathcal{Z}_k(J) = \int \mathcal{D}x \exp \left[-\mathcal{S}[x] - \Delta \mathcal{S}_k[x] + \int_t Jx \right] \quad (35)$$

where the regulating term $\Delta \mathcal{S}_k[x]$ is quadratic in x :

$$\Delta \mathcal{S}_k[x] = \frac{1}{2} \int_{t,t'} x(t) R_k(t, t') x(t') \quad (36)$$

Crucially R_k is an IR regulator that depends on a Renormalisation scale k and the momentum p of the modes. The precise form of R_k is not crucially important and it is chosen in order to optimize calculations but it should satisfy $\lim_{k \rightarrow 0} R_k = 0$, ensuring that the full effective action (33) is recovered in this limit.

By defining the mean position as before $\chi(t) \equiv \langle x(t) \rangle$ we can construct the Regulated Effective Action:

$$\Gamma_k[\chi] = \int_t J\chi - \mathcal{W}_k[J] - \Delta \mathcal{S}_k[\chi] \quad (37)$$

where $\mathcal{W}_k[J] = \ln(\mathcal{Z}_k)$ is analogous to the non-regulated case.

From the Regulated Effective Action one can obtain obtain the Wetterich equation [7]:

$$\partial_k \Gamma_k[\chi] = \frac{1}{2} \int_{t,t'} \partial_k R_k(t, t') \left[R_k + \Gamma_k^{(2)} \right]^{-1} \quad (38)$$

which is a functional equation determining how Γ_k changes as $k \rightarrow 0$. It interpolates Γ_k from the microscopic scale ($k = \Lambda$), where $\Gamma_\Lambda = \mathcal{S}$, down to the IR regime ($k = 0$) where the full effective action $\Gamma[\chi] = \Gamma_{k=0}[\chi]$, encoding the effect of all fluctuations, is obtained. A simplified derivation for one degree of freedom at equilibrium, which however captures all the relevant manipulations, can be found in appendix C.

As demonstrated in the previous section, our Brownian motion problem is actually SUSY QM. We can therefore apply the fRG technology and incorporate the effect of thermal fluctuations by following the flow of the effective action Γ_k via the Wetterich equation. The relevant flow equations for this system have been derived in Synatschke et. al [18] whose results we adopt here.

A. Local Potential Approximation

In practice, calculating Γ_k exactly is usually impossible and we must consider a truncation to make the functional equation (38) tractable. The Local Potential Approximation (LPA) is the assumption that the only part of the effective action that depends on our momentum scale k is the superpotential W . Synatschke et. al therefore pick an effective action of the form:

$$\begin{aligned} \Gamma_k[\phi, F, \bar{\psi}, \psi] = \int d\tau \left[\frac{1}{2} \dot{\phi}^2 + \frac{1}{2} F^2 + iFW_{k,\phi}(\phi) \right. \\ \left. - i\bar{\psi} (\partial_t + W_{k,\phi\phi}) \psi \right] \end{aligned} \quad (39)$$

such that $\Gamma_{k=\Lambda} = \mathcal{S}_{SUSY}$ under the condition $W_{k=\Lambda}(\phi) = W(\phi)$ with $\phi \equiv \langle \varphi \rangle$ being the mean field. In this approximation the only thing changing with k directly, progressively incorporating the effect of fluctuations on different timescales, is W_k . This means we only have one flow equation to solve which turns out to be:

$$\partial_k W_k(\phi) = \frac{1}{2} \int_{-\infty}^{\infty} \frac{dp}{2\pi} \frac{\partial_k r_1}{p^2 + (r_1 + \partial_{\phi\phi} W_k(\phi))^2} \quad (40)$$

where r_1 is a regulator subject to the appropriate conditions to match the UV action: suppress IR modes and vanish as $k \rightarrow 0$. We will use the simplest regulator that satisfies these conditions, the Callan-Symanzik regulator $r_1 = k$ which gives us the very simple flow equation:

$$\partial_k W_k(\phi) = \frac{1}{4} \cdot \frac{1}{k + \partial_{\phi\phi} W_k(\phi)} \quad (41)$$

or, in terms of our physical parameters x and V :

$$\partial_k V_k(\chi) = \frac{\Upsilon}{2} \cdot \frac{1}{k + \varepsilon \cdot \partial_{\chi\chi}^2 V_k(\chi)} \quad (42)$$

where $\Upsilon \equiv k_b T/m$ determining the thermal energy of the system per mass of the particle. This is the fundamental flow equation under the Local Potential Approximation.

It is convenient to rescale $k \rightarrow \varepsilon \tilde{k}$ such that the LPA PDE takes the form:

$$\partial_{\tilde{k}} V_{\tilde{k}}(\chi) = \frac{\Upsilon}{2} \cdot \frac{1}{\tilde{k} + \partial_{\chi\chi}^2 V_{\tilde{k}}(\chi)} \quad (43)$$

i.e. we have scaled out the small parameter ε in the denominator which is numerically hazardous. This equation can then be discretised in the χ direction and become a set of coupled ODEs that can be solved in the \tilde{k} direction in order to obtain a numerical solution. Note that due to the rescaling $\tilde{k} \in [0, \Lambda/\varepsilon]$.

B. Wave Function Renormalisation

In the previous subsection we assumed that the effective action Γ_k only depends on the renormalisation scale through the form of the potential. We now allow for the field φ itself to be renormalised which results in a scaling of the kinetic term. The new effective action in the SUSY formalism is [18]:

$$\Gamma_k[\phi, \bar{\psi}, \psi] = \int dt \frac{1}{2} Z_{,\phi}^2 \dot{\phi}^2 + \frac{1}{2} \left(\frac{W_{,\phi}}{Z_{,\phi}} \right)^2 - i\bar{\psi} \left(Z_{,\phi}^2 \partial_t + Z_{,\phi} Z_{,\phi\phi} \dot{\phi} - Z_{,\phi\phi} \frac{W_{,\phi}}{Z_{,\phi}} + W_{,\phi\phi} \right) \psi \quad (44)$$

where we have suppressed the explicit dependence on k of W & Z to avoid overly cluttered notation. From now on we will in general drop this explicit dependence on k for W , V , Z & ζ , defined below, only restoring it when

we are directly comparing it to the original cutoff value. We introduce an additional identification in addition to (24):

$$\zeta(x) = \sqrt{2D} Z(\phi) \Rightarrow \zeta_{,x} = Z_{,\phi} \quad (45)$$

$$\bar{c}c = -i\zeta_{,x} \bar{\psi}\psi \quad (46)$$

such that the (on-shell) effective action for Brownian motion is now written as:

$$\Gamma_k[\chi, \bar{c}, c] = \int dt \frac{1}{4D} \zeta_{,\chi}^2 \dot{\chi}^2 + \frac{\varepsilon^2}{4D} \left(\frac{V_{,\chi}}{\zeta_{,\chi}} \right)^2 - \bar{c} \left(\zeta_{,\chi}^2 \partial_t + \zeta_{,\chi} \zeta_{,\chi\chi} \dot{\chi} - \varepsilon \cdot \zeta_{,\chi\chi} \frac{V_{,\chi}}{\zeta_{,\chi}} + \varepsilon \cdot V_{,\chi\chi} \right) c \quad (47)$$

The regulator term becomes more complicated for this action and we do not reproduce it here, see [18] for details of this. Following their approach one arrives at the LPA + WFR flow equations:

$$\partial_{\tilde{k}} V_{\tilde{k}}(\chi) = \frac{\Upsilon}{2} \cdot \frac{1}{\tilde{k} + \partial_{\chi\chi}^2 V_{\tilde{k}}(\chi)} \quad (48)$$

$$\partial_{\tilde{k}} \zeta_{,\chi} = \frac{\Upsilon}{2} \cdot \frac{\mathcal{P}}{\zeta_{,\chi} \cdot \mathcal{D}} \quad (49)$$

$$\mathcal{D} \equiv V_{,\chi\chi} + \tilde{k} \zeta_{,\chi}^2 \quad (50)$$

$$\mathcal{P} \equiv \frac{4\zeta_{,\chi\chi} V_{,\chi\chi\chi}}{\mathcal{D}} - (\zeta_{,\chi\chi} \zeta_{,\chi})_{,\chi} - \frac{3\zeta_{,\chi}^2 V_{,\chi\chi\chi}^2}{4\mathcal{D}^2} \quad (51)$$

which now consist of the previous LPA equation for the effective potential (43) as expected, augmented by one more flow equation for the wavefunction renormalization $\zeta_{,\chi}$.

We will integrate the LPA equation (43) by discretising along the χ direction and solving the resulting set of coupled ODEs in k . Once the effective potential $V_k(\chi)$ has been obtained the second PDE can be solved for $\zeta_{,\chi}$ in a similar way. It is worth pointing out here that our approach differs slightly from [18] in that the effective potential obeys the same equation as in the LPA approximation even with the inclusion of WFR.³ This is because the equilibrium state is described exactly by the LPA equation [17, 21, 22], as we explicitly show in appendix C. The LPA flow equation was first solved in [18, 21, 22], while more recently WFR was included for a double well potential in [17].

IV. OBSERVABLES

One of the benefits of the fRG formalism is that the object at its focus, the effective action $\Gamma[\chi]$, can be used to extract observable quantities in a relatively straightforward manner. In this work we focus on the 1-point and

³ The regulator used in [18] in the WFR approximation leads to deviations from the correct equilibrium position and variance.

2-point connected correlation functions, or Ursell functions, at equilibrium. In what follows we discuss how they can be obtained from knowledge of the effective action $\Gamma[\chi]$, also giving a brief account on how higher order functions could be calculated.

A. 1-point function

The first functional derivative of $\Gamma_{k=0}$ gives us the effective equation of motion for the mean position $\chi(t) = \langle x(t) \rangle$. Under the LPA:

$$\frac{\delta\Gamma_{k=0}}{\delta\chi(t)} = \ddot{\chi} - \varepsilon^2 \partial_\chi V_{k=0}(\chi) \partial_{\chi\chi}^2 V_{k=0}(\chi) = 0 \quad (52)$$

where the final equality comes by assuming that source terms have been set to zero (i.e $J(t) = 0$). The WFR version of the effective equation of motion reads

$$(\zeta_{,\chi}\dot{\chi}) \cdot -\varepsilon^2 \frac{\partial_\chi V_{k=0}}{\zeta_{,\chi}^2} \left(\partial_{\chi\chi}^2 V_{k=0} - \frac{\zeta_{,\chi\chi}}{\zeta_{,\chi}} \partial_\chi V_{k=0} \right) = 0 \quad (53)$$

where $\partial_\chi \zeta$ and $\partial_\chi^2 \zeta$ are also evaluated at $k = 0$. Equilibrium is defined for both LPA & WFR by the condition

$$\partial_\chi V_{k=0}(\chi_{eq}) = 0 \quad (54)$$

As the potential $V_{k=0}(\chi)$ should be convex (by definition of Γ) equation (54) tells us that χ_{eq} corresponds to the minimum of $V_{k=0}(\chi)$. Or more concretely:

$$\lim_{t \rightarrow \infty} \langle x(t) \rangle = x \text{ that minimises } V_{k=0}(x) \quad (55)$$

This is exactly as one would intuitively think by looking at the shapes of $V_{k=0}$ – see section V. The equilibrium position is obviously the same for both LPA and WFR.

B. 2-point function

The connected 2-point function $G(t, t') = \langle x(t_1)x(t_2) \rangle_C = \delta^2 \mathcal{W} / \delta J(t_1) \delta J(t_2)$ and the second functional derivative of the effective action $\Gamma_{k=0}$ are inverse to each other

$$\int d\tau \frac{\delta^2 \Gamma_{k=0}}{\delta\chi(t) \delta\chi(\tau)} \frac{\delta^2 \mathcal{W}_{k=0}}{\delta J(\tau) \delta J(t')} = \delta(t - t') \quad (56)$$

Assuming that equilibrium has been reached, the above relation reads more concretely

$$\left(\frac{d^2}{dt^2} - \varepsilon^2 \lambda^2 \right) G(t_1, t_2) = -2\Delta \delta(t_2 - t_1) \quad (57)$$

where

$$\lambda^2 \equiv \begin{cases} V_{,\chi\chi}^2, & \text{for LPA} \\ \frac{V_{,\chi\chi}^2}{\zeta_{,\chi}^4}, & \text{for WFR} \end{cases} \quad (58)$$

and

$$\Delta \equiv \begin{cases} D, & \text{for LPA} \\ \frac{D}{\zeta_{,\chi}^2}, & \text{for WFR} \end{cases} \quad (59)$$

The notation $|$ means we have evaluated the function at $k = 0$ and at equilibrium $\chi = \chi_{eq}$.

The appropriate solution to (57) providing the connected correlation function at equilibrium is

$$\langle x(t_1)x(t_2) \rangle_C = \frac{\Upsilon}{V_{,\chi\chi}} e^{-\varepsilon\lambda|t_1-t_2|} \quad (60)$$

$$\Rightarrow \langle x^2 \rangle_C = \frac{\Upsilon}{V_{,\chi\chi}} \quad (61)$$

Equation (61) gives us a direct way to calculate the variance of the distribution at equilibrium from the computed effective potential. In the LPA approximation the variance and the decay rate of the autocorrelation function are both directly given by the curvature of the effective potential at its minimum. The inclusion of WFR however alters the decay rate without changing the equilibrium variance. This is as it should since the latter is fixed by the equilibrium Boltzmann distribution. As we will see in section V, where explicit results for various potentials are given, WFR improves the decay rate which is indeed not exactly determined by the effective potential's curvature.

C. Connected 3- & 4-point functions

It is straightforward to generalise the above treatment to higher point functions in the fRG formalism. The connected and 1PI correlation functions can be calculated in a standard way (see for e.g. pg 381-382 of [5]). Assuming that $t_4 \geq t_3 \geq t_2 \geq t_1$ then the 3-point function for example is:

$$\langle x(t_1)x(t_2)x(t_3) \rangle_C = \langle x(t_1)^3 \rangle_C e^{-\varepsilon\lambda(2t_3-t_2-t_1)} \quad (62)$$

$$\langle x(t_1)^3 \rangle_C \equiv -\langle x(t_1)^2 \rangle_C^3 \frac{\mathcal{V}_{,\chi\chi\chi}}{3\varepsilon\lambda} \quad (63)$$

Where we have introduced the notion of the *bosonic potential* \mathcal{V} :

$$\mathcal{V}(k, \chi) \equiv \begin{cases} V_{,\chi}^2(k, \chi), & \text{for LPA} \\ \frac{V_{,\chi}^2(k, \chi)}{\zeta_{,\chi}^2(k, \chi)}, & \text{for WFR} \end{cases} \quad (64)$$

Similarly the 4-point function is:

$$\langle x(t_1)x(t_2)x(t_3)x(t_4) \rangle_C = \langle x(t_1)^4 \rangle_C e^{-\varepsilon\lambda(3t_4-t_3-t_2-t_1)} \quad (65)$$

$$\langle x(t_1)^4 \rangle_C \equiv \frac{\langle x(t_1)^2 \rangle_C^4}{4\varepsilon\lambda} \left(\mathcal{V}_{,\chi\chi\chi}^2 \frac{\langle x(t_1)^2 \rangle_C}{\varepsilon\lambda} - \mathcal{V}_{,\chi\chi\chi\chi} \right) \quad (66)$$

From these connected correlation functions one should be able to calculate the skewness and kurtosis of the equilibrium distribution in a similar manner to what we did for χ_{eq} and $\mathbf{Var}(x)$. We leave this calculation and comparison to the Boltzmann distribution for future work.

V. RESULTS

In this section we numerically integrate the flow equations, obtaining the resulting effective potential and wave function renormalization for the three types of potentials mentioned in the introduction. The minima of the LPA effective potentials determine the equilibrium position of the particle in each case and their curvature at the minimum determines the variance. We find excellent agreement with the values obtained by the Boltzmann equilibrium distribution, allowing us to establish the accuracy of our numerical solution for the LPA flow equation. In the LPA approximation, the effective potentials' curvatures also determine the decay rates of the autocorrelation functions in equilibrium. We compare these with high accuracy numerical simulations of the stochastic process done using the open source software Large-scale Atomic/Molecular Massively Parallel Simulator (LAMMPS). We find poorer agreement with the LPA prediction alone but the decay rates also receive a correction from wavefunction renormalization. We find that, when wavefunction renormalization is included, the autocorrelation decay rates for the potentials we study are quantitatively predicted by the fRG at the percent level.

A. Solutions to the flow equations

1. Polynomial Truncation

Before solving the full PDE (43) it is instructive to consider an approximation, focusing on the double well potential (7) for illustration. We consider a truncated polynomial ansatz for the effective potential $V_k(\chi)$ of the form

$$V_k(\chi) = E(k) + \sum_{i=1}^N \alpha_i(k) \chi^{2i} \quad (67)$$

with initial conditions defined such that it matches the original doublewell potential (7) at the cutoff:

$$E(k = \Lambda) = 0 \quad (68)$$

$$\alpha_1(k = \Lambda) = a \quad (69)$$

$$\alpha_2(k = \Lambda) = b \quad (70)$$

and all coefficients of higher powers vanishing. We can then expand the r.h.s of (43) in powers of χ , truncate the series at $2N$ and therefore write a set of $N + 1$ coupled ODEs in terms of the couplings that can then be solved

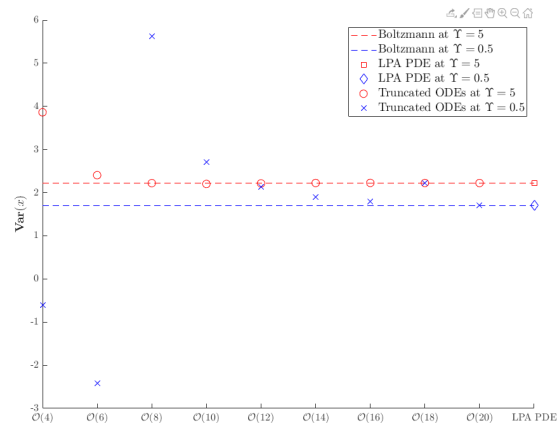


FIG. 1: The convergence of the truncated system of ODEs to the full LPA PDE value for $\mathbf{Var}(x)$ at equilibrium for $\Upsilon = 5$ (red) and $\Upsilon = 0.5$ (blue). $\mathbf{Var}(x)$ as calculated from the Boltzmann distribution is also included for reference

numerically. Below we write the set of ODEs for the $\mathcal{O}(4)$ truncation as it only concerns coupling coefficients up to order x^4 :

$$\frac{dE(k)}{dk} = \frac{\Upsilon}{2} \cdot \left(\frac{1}{k + 2\varepsilon \cdot \alpha_1(k)} - \frac{1}{k} \right) \quad (71)$$

$$\frac{d\alpha_1(k)}{dk} = -\frac{6D \cdot \alpha_2(k)}{(k + 2\varepsilon \cdot \alpha_1(k))^2} \quad (72)$$

$$\frac{d\alpha_2(k)}{dk} = \frac{72\varepsilon D \cdot \alpha_2^2(k)}{(k + 2\varepsilon \cdot \alpha_1(k))^3} \quad (73)$$

These equations show how the coefficients in the polynomial ansatz for the potential evolve when fluctuations of lower and lower frequencies are averaged over. Keeping more terms in the polynomial truncation is straightforward, leading to a hierarchy of flow equations for the different coefficients that can be easily obtained via a computer algebra software. Solving such polynomial flow equations is numerically much easier than solving the full PDE (43) and the solution to the full PDE should be approached as $N \rightarrow \infty$. However, this method is only well suited to initial potentials of polynomial form of small degree (e.g. the doublewell $-x^2 + x^4/4$). For potentials with more complex shapes the full PDE must be solved.

The system of ODEs at each truncation was solved using Matlab's built in ode23s function which is based on a modified Rosenbrock formula of order 2. Using equation (61) we can rewrite the variance as: $\mathbf{Var}(x) = \Upsilon/2\alpha_1(k=0)$ thus showing naturally how our coupling constants relate to physical quantities – the variance is inversely proportional to $\alpha_1(k=0)$. The results of this procedure for the doublewell potential are displayed in Fig. 1. Here we can see that the lowest order truncations match poorly with the correct value as given by the Boltzmann distribution. This discrepancy being particularly

noticeable for $\Upsilon = 0.5$ with predictions of negative variance which is unphysical. However the value calculated by solving the full LPA PDE (43) is approached by including more terms with the $\mathcal{O}(20)$ truncation matching the full PDE at both temperatures. Setting the energy gap for the doublewell to be $\Delta E = m$ means that choosing $\Upsilon = 1$ corresponds to a thermal energy equal to the height barrier. We can therefore also think of $\Upsilon > 1$ corresponding to low barriers and $\Upsilon < 1$ to high barriers.

We see that, in this example at least, the polynomial approximation to the flow equations offers a viable option to solving the flow, with the added bonus that it can be solved much quicker than the full LPA PDE. However, if the initial potential is not well approximated by a polynomial such as the Unequal-Lennard Jones then one is forced to solve the full LPA PDE. Furthermore, computing the autocorrelation decay rate requires one to go beyond the LPA and include WFR, doubling the complexity of any polynomial truncation. It is also believed that to get sensible results for quantities out of equilibrium we need to solve the full PDE – we explore this in more detail in our upcoming companion paper concerning non-equilibrium phenomena. We therefore now turn to the full PDEs, the numerical solution to which is feasible and accurate as we demonstrate.

2. Full PDEs

We solve the LPA flow equation (43) on a grid in the χ direction, using Matlab's built in ode45 or ode15s function to evolve in the k direction, depending on the potential. For most potentials ode45 – which is based on an adaptive step size Runge-Kutta method – was sufficient. A similar approach was used for including (49). The numerical derivatives in the χ direction were based on a finite difference scheme using the Fornberg method with a stencil size of 5 for the potentials under study. While increasing the grid size improves the accuracy of the numerical derivative it also increases the number of coupled ODEs to be solved, making the integration much more computationally expensive. A balance must be drawn depending on the potential in question. We considered 1001 points with $x \in (-3, 3)$ for the ULJ and $x \in (-5, 5)$ for the rest.

Our first example of a flow from the bare to the effective potential for high and low temperature, $\Upsilon = 5$ and $\Upsilon = 0.5$ respectively, is shown in Fig. 2 involving a polynomial potential. The flow in the range $k \in (0.01, 600)$ is rather inconsequential and there is not much change in the shape of the potential. As $k \rightarrow 0$ is approached however, a distinct single minimum develops indicating the average position of the particle. As expected, the lower the temperature, the closer the effective minimum is to the bare potential's minimum, indicating the rela-

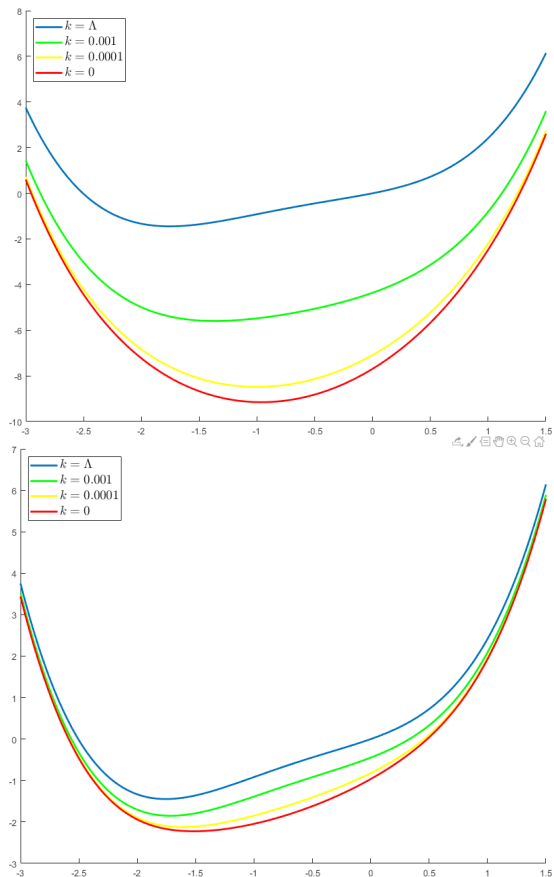


FIG. 2: The flow of the polynomial Langevin potential V in the LPA for $\Upsilon = 5$ (top) and $\Upsilon = 0.5$ (bottom). The blue curve indicates the bare potential which is progressively changed, through green and yellow, into the red effective potential, as fluctuations are integrated out.

tive weakness of fluctuations to force the particle to spend time away from it.

A perhaps more interesting case is shown in Fig. 3, displaying how the double well potential flows with renormalisation scale k to its effective incarnation for high $\Upsilon = 5$ and low $\Upsilon = 0.5$ temperature. Again, for the high temperature in the range $k \in (0.01, 600)$ there is not much change in the shape of the potential. Physically this means that the fluctuations we have integrated out in this range do not contribute significantly to the particle moving between the two minima, only displacing the particle about each of the two distinct minima. However, by $k = 0.001$ the energy barrier has gotten significantly smaller meaning that we have started to integrate over fluctuations that drive the particle over the barrier. Naturally, when $k = 0$ is reached the potential is fully convex (as it must be by definition of Γ) with no barriers to overcome. Similar behaviour is obtained where again we consider the lower temperature, $\Upsilon = 0.5$. As one might expect it takes 'longer' in k evolution for

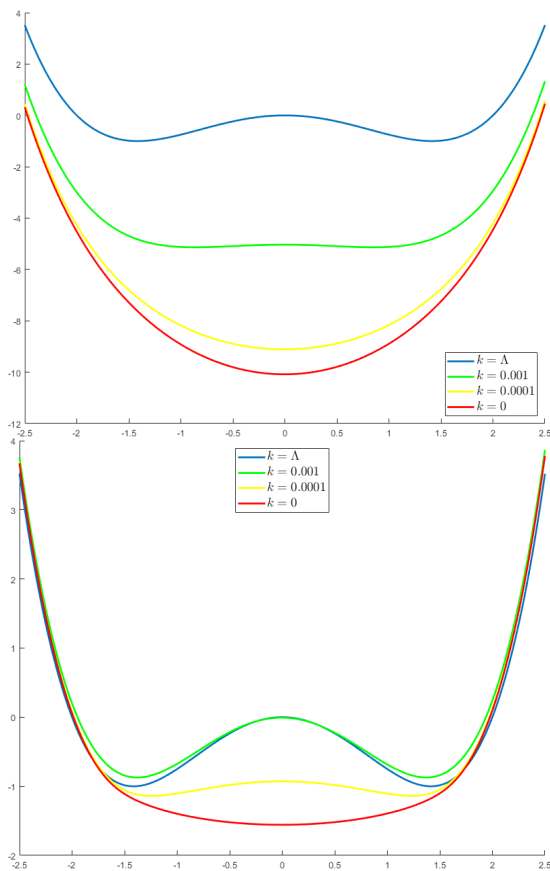


FIG. 3: The flow of the doublewell Langevin potential V in the LPA for $\Upsilon = 5$ (top) and $\Upsilon = 0.5$ (bottom). The blue curve indicates the bare potential which is progressively changed, through green and yellow, into the red effective potential, as fluctuations are integrated out.

the barrier to disappear as fluctuations at each k scale have less energy than their equivalent for the $\Upsilon = 5$ case. Of note is that not only is the evolution different but the final shape of $V_{k=0}(x)$ is different for the two different temperature regimes. For $\Upsilon = 0.5$ it is clear that the potential is much flatter around the origin than for $\Upsilon = 5$. This is suggestive of longer time scales required at lower temperatures to overcome the energy barrier and reach equilibrium. It also indicates longer times for the connected 2-point function to decay, as we discuss below.

Also of note is that for both cases the global minimum shifts from its degenerate values at $\pm\sqrt{2}$ to $x = 0$. This makes physical sense as one expects that the particle will spend most of its time at the bottom of each well so that its average position will be in the middle i.e. at the origin. This is suggestive of the fact that the minimum of the fully flowed potential $V_{k=0}(x)$ should correspond to the equilibrium position of the particle at late times. We showed that this is indeed the case in section IV and will verify this numerically.

As our third example we turn to a non-symmetric non-

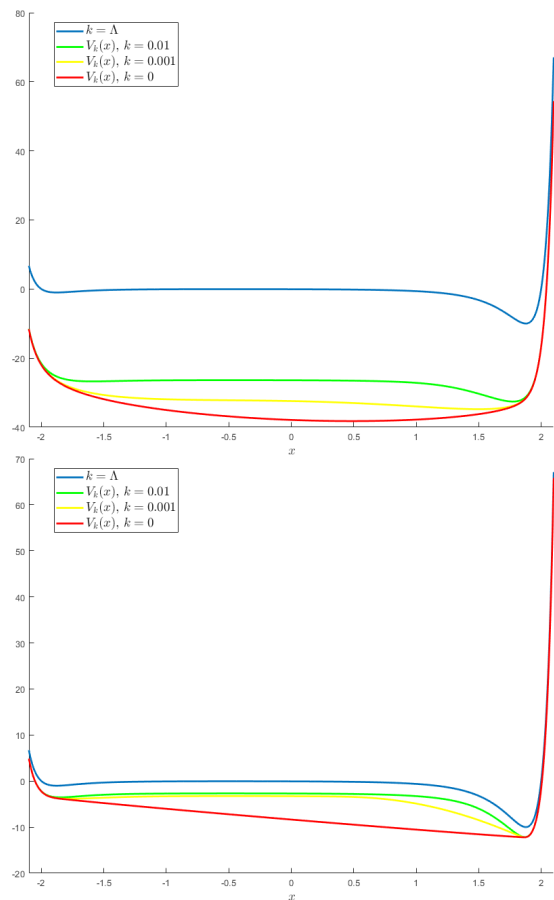


FIG. 4: The flow of the unequal L-J Langevin potential V in the LPA for $\Upsilon = 5$ (top) and $\Upsilon = 0.5$ (bottom). Again, the bare potential is denoted by the blue curve and the $k = 0$ effective potential by the red one.

polynomial potential. Fig. 4 displays the evolution with k for an Unequal double Lennard-Jones (ULJ) potential under the LPA for high ($\Upsilon = 5$) and low ($\Upsilon = 0.5$) temperature. Similarly to the double well case the energy barriers get smaller and eventually disappear as k is lowered and $V_{k=0}$ is fully convex. As one might expect however, $V_{k=0}$ is not symmetric but the minimum of $V_{k=0}$ does not match the global minimum initially. The new global minimum is a $x > 0$ which is suggestive that the particle spends most of its time in the deeper well on the right but still spends a significant amount of time in the smaller well such that the average position at late times lies in between the two. This does not appear to be the case for $\Upsilon = 0.5$ as shown in the bottom plot of Fig. 4. Here the minimum at $k = 0$ is very close to the original global minimum, suggesting that the particle can nearly always be found here at equilibrium. This makes sense because as the temperature is lowered the particle is more likely to be found in the global minimum as it has less energy to escape and explore its surroundings. We expand on this idea more in the next subsection.

Including WFR does not change the evolution or final shape of $V_k(x)$ but adds one more function $\zeta_{,x}$ to be

evolved in k . Its evolution with k for the three types of potential is shown in Figs. 5, 6 and 7. At the start of the flow (blue curves) $\zeta_x = 1$ with a non-trivial χ dependence developing as $k \rightarrow 0$, shown by the red curve. Similar to the potential, as k is lowered it takes longer for changes to happen. $\zeta_x(x)$ at $k = 0$ for $\Upsilon = 0.5$ is much flatter than for $\Upsilon = 5$. The evolution of $\zeta_x(x)$ with k for the unequal L-J potential is shown in Fig. 7. The behaviour is similar to the doublewell case except now it is not symmetric with a larger peak for $x > 0$ as one might expect considering the initial shape of V . The origin of these peaks is clear for the doublewell and unequal L-J potential. In both cases they form around the local minima of the bare V potential, e.g. for the doublewell this is at $x = \pm\sqrt{2}$ which we can see matches the peak of the red curves in Fig. 6.

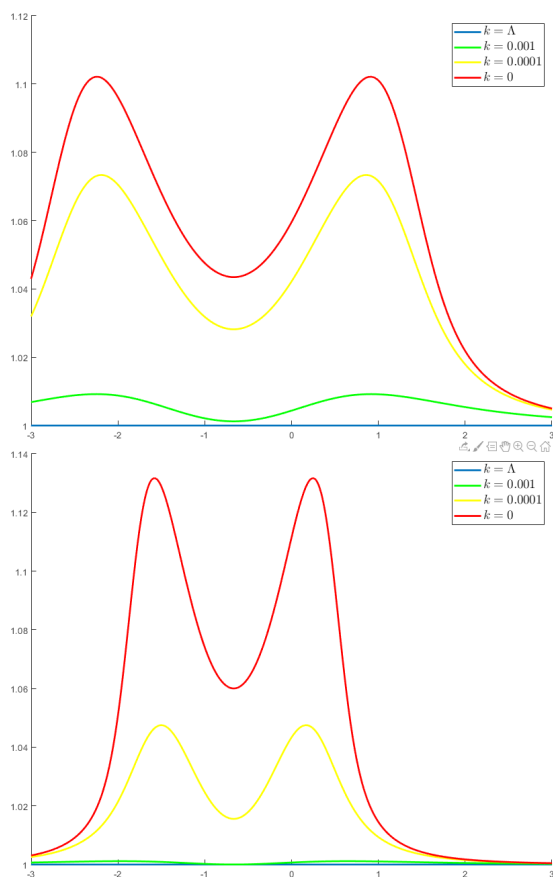


FIG. 5: The flow of ζ_x in polynomial potential for $\Upsilon = 5$ (top) and $\Upsilon = 0.5$ (bottom)

It is perhaps not surprising that including the running of ζ_x seriously complicates the numerics of the problem, equation (49) is more complicated than (43), however the effect is significant. For example we were unable to obtain stable numerics for the evolution of ζ_x in the unequal L-J potential for $\Upsilon = 0.5$ hence its omission. The calculations for ζ_x also take significantly longer than for V_k

alone as much smaller timesteps are required to be within acceptable numerical tolerances. As an example the calculation of V_k for the unequal L-J took ~ 5 minutes on a simple desktop machine whereas also calculating ζ_x on the same machine took several hours. With more specialist numerical integrators tailor made for these equations it is conceivable that computations could be done quicker and ζ_x could be calculated for potentials and temperatures currently inaccessible using proprietary software. We leave this to future work.

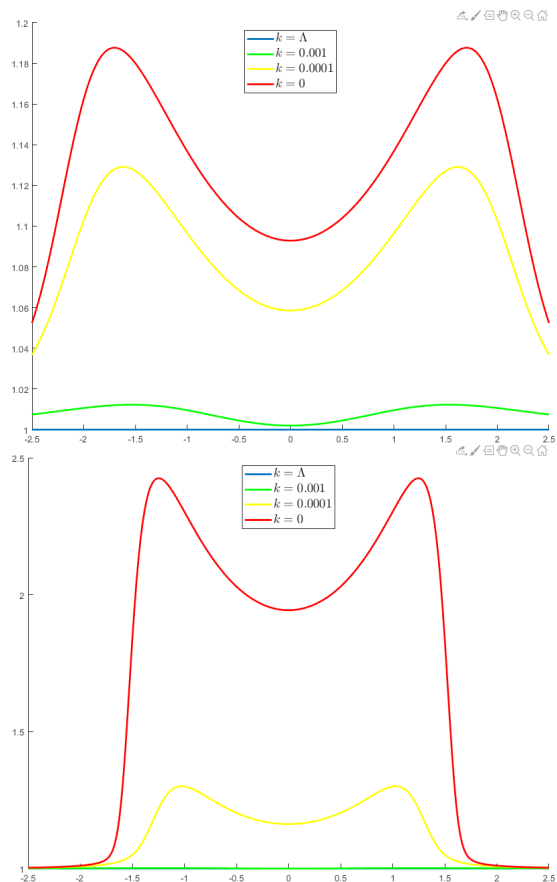


FIG. 6: The flow of ζ_x for the double well potential for $\Upsilon = 5$ (top) and $\Upsilon = 0.5$ (bottom)

B. Equilibrium position

As we discussed in section IV and saw in the previous subsection, the minimum of the effective potential at $k = 0$ should correspond to the average position of the particle in equilibrium. Here we verify that this is indeed the case by comparing the position of these minima to what we would expect from the Boltzmann distribution. Let us consider the (normalised) equilibrium Boltzmann

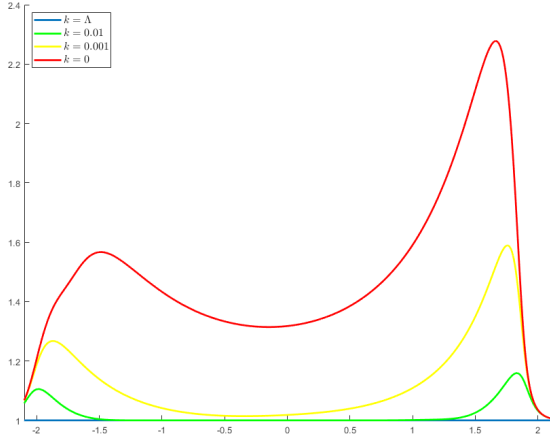


FIG. 7: The flow of ζ_x in an unequal L-J potential under WFR for $\Upsilon = 5$.

distribution (which also relates to the eigenfunction of the zero eigenvalue mode $E_0 = 0$ of the Schroedinger equation (B8)) defined in the standard way:

$$P(x) = N \exp\left(-\frac{V(x)}{\Upsilon}\right) \quad (74)$$

where N is chosen so that $\int_{-\infty}^{\infty} P(x) = 1$. We can then compute χ_{eq} in the standard way from the equilibrium probability distribution function:

$$\int_{-\infty}^{\infty} x \cdot P(x) = \chi_{eq} \quad (75)$$

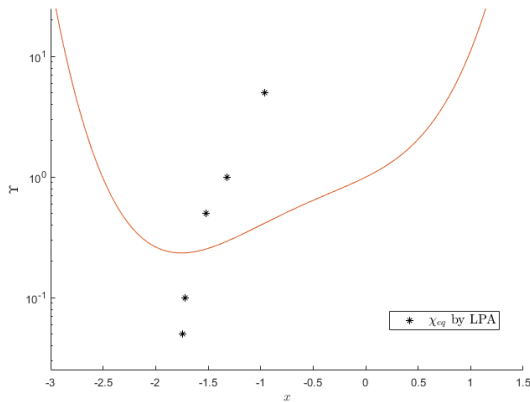


FIG. 8: The value of χ_{eq} for different values of Υ in the polynomial potential as calculated via the LPA. The original bare polynomial Langevin potential is plotted (not to scale) in red for context

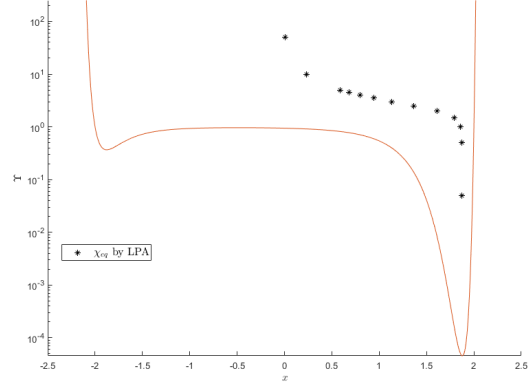


FIG. 9: The value of χ_{eq} for different values of Υ in the Unequal Lennard-Jones potential as calculated via the LPA. The original bare unequal Lennard-Jones type Langevin potential is plotted (not to scale) in red for context

Looking at Table. I we can see that the LPA matches the Boltzmann distribution extremely well for a wide range of different potentials. In Figs. 8 & 9 we have plotted the LPA prediction for the average position as the thermal energy Υ of the system is lowered and the equilibrium position shifts closer to the original potential’s minimum. This is particularly stark in Fig. 9 as it is clear at high temperature the equilibrium position is in the middle of the two wells suggesting a roughly symmetric Boltzmann distribution. However as temperature is lowered the χ_{eq} moves into the deeper well indicating that particles at equilibrium at low temperatures would nearly always be in this region as one would expect. Table I verifies that the LPA properly captures this crucial physical aspect of the system at equilibrium and that, indeed, the numerical solution to the LPA equation is indeed accurate.

| Potentials | Υ | Boltz | LPA |
|-------------|------------|---------|--------|
| Polynomial | 5 | -0.9618 | -0.96 |
| | 0.5 | -1.5170 | -1.52 |
| Unequal L-J | 5 | 0.4854 | 0.485 |
| | 0.5 | 1.8684 | 1.87 |
| Rugged - | 5 | -0.9618 | -0.96 |
| Polynomial | 0.5 | -1.5170 | -1.52 |
| Rugged - | 5 | 0.5010 | 0.50 |
| Unequal L-J | 0.5 | 1.8499 | 1.8575 |

TABLE I: χ_{eq} as calculated from the Boltzmann distribution and the LPA effective potential.

C. Variance

The fRG also allows for the computation of the *variance* of the equilibrium distribution, defined by:

$$\int_{-\infty}^{\infty} (x - \chi_{eq})^2 \cdot P(x) = \mathbf{Var}(x) \quad (76)$$

with the fRG predicting it to be

$$\mathbf{Var}(x) = \langle x^2 \rangle_C \stackrel{(61)}{=} \frac{\Upsilon}{V_{,xx}} \quad (77)$$

Clearly, the variance is related to how flat the potential is near $k = 0$, controlled by $V_{,xx}$ at the equilibrium point. Unsurprisingly, the bigger the curvature of the effective potential, the smaller the variance for a fixed temperature.

Once the fRG flow equations have been solved, calculating the the effective potential's curvature at the minimum is very straightforward. Our results are summarised in Table. II and it is clear that the LPA offers very good agreement for the variance of the equilibrium distribution for all the potentials examined. Conversely, this again demonstrates that the numerical solution to the LPA equation is accurate.

| Potentials | Υ | Boltz | LPA |
|-------------|------------|------------------------|-------------------------|
| Doublewell | 5 | 2.2198 | 2.2199 |
| | 0.5 | 1.7043 | 1.7042 |
| Polynomial | 5 | 1.5690 | 1.5695 |
| | 0.5 | 0.2938 | 0.2922 |
| Unequal L-J | 5 | 1.6858 | 1.6860 |
| | 0.5 | $1.0809 \cdot 10^{-3}$ | $1.02726 \cdot 10^{-3}$ |
| Rugged - | 5 | 2.2198 | 2.2199 |
| Doublewell | 0.5 | 1.7043 | 1.7042 |
| Rugged - | 5 | 1.5690 | 1.5695 |
| Polynomial | 0.5 | 0.2938 | 0.2948 |
| Rugged - | 5 | 1.6818 | 1.6825 |
| Unequal L-J | 0.5 | $7.2618 \cdot 10^{-4}$ | $6.9456 \cdot 10^{-4}$ |

TABLE II: $\mathbf{Var}(x)$ as calculated from the Boltzmann distribution and the LPA effective potential.

D. Connected 2-point function

In addition to the static variance at equilibrium, the flatness of the effective potential around the minimum also determines the time dependence of correlations in equilibrium, quantified by the time dependent covariance or connected 2-point function

$$\langle x(t_1)x(t_2) \rangle_C = \frac{\Upsilon}{V_{,xx}} e^{-\varepsilon\lambda|t_2-t_1|} \quad (78)$$

where λ is given by (58). In Table. III we collect the values of λ obtained using the fRG under LPA & WFR for $\Upsilon = 5$ and $\Upsilon = 0.5$ and compare this directly to High

accuracy numerical simulations of the Langevin equation (4) using LAMMPS. Where possible we also computed the first non-zero eigenvalue E_1 by diagonalising the Hamiltonian from the Schrodinger equation in (B4). We can clearly see from Table. III that for our potentials the value obtained via the LPA tends to deviate by $\sim 10\% - 15\%$ from the simulation value. However, inclusion of the WFR factor $\zeta_{,x}$ reduces the deviation substantially error to $\sim 1\% - 3\%$ from the value obtained in the simulations.

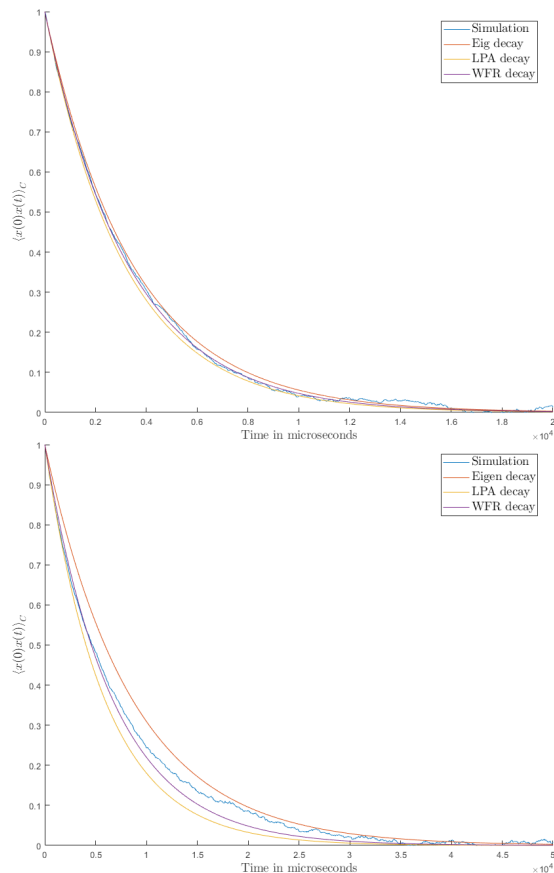


FIG. 10: The decay of the (normalised) connected two point function $\langle x(0)x(t) \rangle_C$ at equilibrium in a polynomial potential for $\Upsilon = 5$ (top) and $\Upsilon = 0.5$ (bottom)

We plot the decay of the connected 2-point function for our three potentials of interest in Figs. 10, 11 & 12 at both high and low temperatures as calculated by fRG techniques compared to direct numerical simulations of the langevin equation. For a polynomial potential, as shown in Fig. 10, we can see how the decay rate as calculated via the fRG for both LPA and LPA + WFR closely matches the simulations at both high and low temperature. Fig. 11 shows the decay in the doublewell which at high temperature (top plot) shows great agreement with the simulation and Schrodinger calculation of λ with fRG methods. At lower temperature (bottom plot)

of Fig. 11 however we can see that the LPA is poorly capturing the correct decay rate and the improvement including WFR offers is much more dramatic. The calculation of E_1 from the Schrodinger equation is a non-trivial numerical exercise for our unequal Lennard-Jones potential hence its omission from Table. III and Fig. 12. Here the fRG offers a very real advantage over more conventional methods to calculating this decay rate as we do not have to develop special numerical routines for every potential of interest, we simply solve the same two flow equations (43) & (49). We can see in Fig. 12 how the LPA + WFR decay rate closely matches the simulated decay at high temperature with the advantage of being calculated much more quickly than the direct simulation. Even just the LPA decay at low temperature as seen in Table. III puts us in the correct ballpark for decay rate.

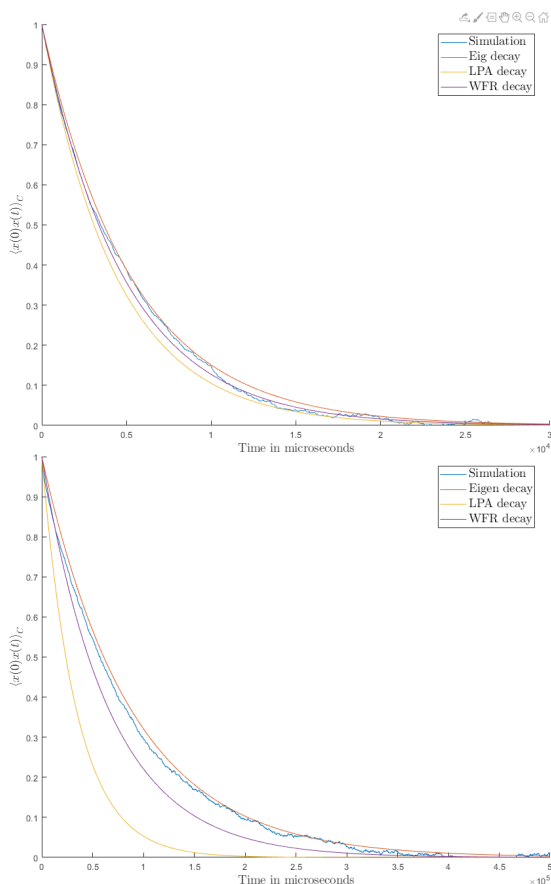


FIG. 11: The decay of the (normalised) connected two point function $\langle x(0)x(t) \rangle_c$ at equilibrium in a doublewell potential for $\Upsilon = 5$ (top) and $\Upsilon = 0.5$ (bottom)

It is also worth pointing out that the simulated decay rate appears to follow the WFR exponential decay at early times before ‘slowing’ down suggesting the true decay might not be a pure exponential at all times. This can be best seen in the bottom plots of Figs. 10 & 11 and

in Fig. 12. This perhaps indicates that the fRG is most accurate over shorter timescales and becomes less accurate over longer time-scales due to the coarse-graining procedure as one might expect.

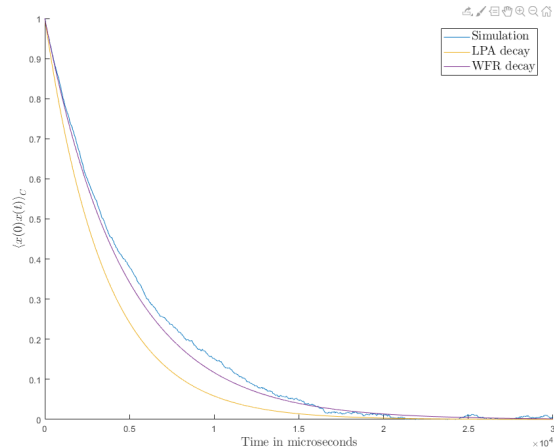


FIG. 12: The decay of the (normalised) connected two point function $\langle x(0)x(t) \rangle_c$ at equilibrium in the ULJ potential for $\Upsilon = 5$

As previously discussed solving the WFR flow equations for more complicated potentials, particularly at low temperature have proved numerically challenging hence the omissions in Table. III. Hopefully with better more custom numerical schemes it would be possible to obtain these values. We leave such calculations to future work.

| Potentials | Υ | LPA | WFR | Sim | $E_1/2$ |
|-------------|------------|----------|---------|---------|---------|
| Doublewell | 5 | 1.1262 | 1.0263 | 0.9940 | 0.9459 |
| | 0.5 | 0.1467 | 0.07269 | 0.06029 | 0.05682 |
| Poly | 5 | 1.5929 | 1.5218 | 1.5041 | 1.4441 |
| | 0.5 | 0.8557 | 0.7579 | 0.6952 | 0.5866 |
| Unequal L-J | 5 | 1.4828 | 1.0410 | 0.9890 | — |
| | 0.5 | 243.3666 | — | 192.672 | — |

TABLE III: Value of the autocorrelation decay rate obtained for various potentials at $\Upsilon = 5, 0.5$ by different methods. The LPA & WFR columns display $\lambda/2$ as calculated from the fRG flow. The simulation values were generated by averaging over 10,000 runs. Note that the difference between the WFR computation and the simulations is systematically smaller than the lowest non-zero eigenvalue of the corresponding Schrodinger equation.

VI. SUMMARY AND DISCUSSION

We have demonstrated how Brownian motion can be formally described by a euclidean path integral involving

a supersymmetric action and how we can calculate the quantum effective action $\Gamma[\chi]$ using functional Renormalisation Group (fRG) methods. The fRG flow equations were written down under two widely used approximations, the Local Potential Approximation (LPA) and the inclusion of Wavefunction Renormalization (WFR). We have shown that a polynomial truncation of the LPA approaches the LPA result after sufficiently many terms. However for initial potentials which are not well approximated by a polynomial solving the full PDE (43) is viable and accurate. We showed that this equation can be solved numerically using standard techniques on a wide variety of potentials and demonstrated the accuracy of the solutions via comparisons to results using the Boltzmann distribution.

The minimum of the effective potential arising as a solution to the LPA flow equation determines the particle's average equilibrium position $\chi_{eq} = \lim_{t \rightarrow \infty} \langle x(t) \rangle$, while the effective potential's curvature at the minimum determines the equilibrium variance $\lim_{t \rightarrow \infty} [\langle x^2(t) \rangle - \langle x(t) \rangle^2]$. The curvature also provides an approximation to the decay rate of the autocorrelation function $\langle x(t)x(0) \rangle$ but with a 10 – 15% error for the potentials we examined. Inclusion of WFR improves the computation of the autocorrelation function significantly, allowing for the determination of the decay rate with an accuracy of $\sim 1 - 3\%$.

In terms of computational effort and speed, the solution of both the LPA and WFR PDEs offer significant advantages over direct numerical simulation of the Langevin equation, averaged over enough realisations to gain accurate statistics. It would be interesting to compare with more established methods involving the Fokker Planck equation, for example in cases where more than one discrete degrees of freedom are involved and especially in field theoretical problems where the Fokker-Planck equation loses its numerical advantage. Finally, it is of interest to examine the utility of the effective action under the LPA and WFR approximations for out-of-equilibrium stochastic dynamics. In a forthcoming, companion paper we apply the fRG to systems displaced from equilibrium and evolving towards it.

ACKNOWLEDGEMENTS

AW would like to thank George Staggs for his numerical insight on solving the flow equations (43) and (49). AW is funded by the EPSRC under Project 2120421. GR would like to thank Nikos Tetradis for very useful discussions at the early stages of this project, Julien Serreau for providing much insight on fRG computations and Gabriel Moreau for sharing his PhD thesis, containing many new results on the application of the fRG to the Langevin equation.

Appendix A: 1-D Langevin equation as radial separation of two particles in 2-D or 3-D

Consider two equal mass particles moving in the same thermal bath with an even⁴ interaction potential between them. The Langevin equations now look like in vector notation:

$$\dot{\vec{x}}_1 + \varepsilon \nabla_{\vec{x}_1} V(\|\vec{x}_1 - \vec{x}_2\|) = \vec{\eta}_1(t) \quad (\text{A1})$$

$$\dot{\vec{x}}_2 + \varepsilon \nabla_{\vec{x}_2} V(\|\vec{x}_2 - \vec{x}_1\|) = \vec{\eta}_2(t) \quad (\text{A2})$$

$$\langle \vec{\eta}_i(t) \vec{\eta}_j(t') \rangle = 2D \delta_{ij} \delta(t - t') \quad (\text{A3})$$

Where \vec{x}_i is a 3D position vector:

$$\vec{x}_i = (x_i, y_i, z_i) \quad (\text{A4})$$

and the choice (A3) is made such that $\eta_i(t)$ is white noise with $D = k_b T / \gamma$ matching the equilibrium Boltzmann distribution. We can now identify our centre of mass vector \vec{X} :

$$\vec{X} \equiv \left(\frac{x_1 + x_2}{2}, \frac{y_1 + y_2}{2}, \frac{z_1 + z_2}{2} \right) = (X, Y, Z) \quad (\text{A5})$$

And spherical polar coordinates in terms of the relative separation of the two particles:

$$x_1 - x_2 = r \cdot \cos \theta \sin \phi \quad (\text{A6})$$

$$y_1 - y_2 = r \cdot \sin \theta \sin \phi \quad (\text{A7})$$

$$z_1 - z_2 = r \cdot \cos \phi \quad (\text{A8})$$

$$r = \sqrt{(x_1 - x_2)^2 + (y_1 - y_2)^2 + (z_1 - z_2)^2} \quad (\text{A9})$$

$$\theta = \arctan \left(\frac{y_1 - y_2}{x_1 - x_2} \right), \quad 0 \leq \theta < 2\pi \quad (\text{A10})$$

$$\phi = \arccos \left(\frac{z_1 - z_2}{r} \right), \quad 0 \leq \phi \leq \pi \quad (\text{A11})$$

We can then rewrite equations (A1) & (A2):

$$\dot{r} + \varepsilon_r \frac{\partial}{\partial r} V(r) = \eta_r(t) \quad (\text{A12})$$

$$\dot{\theta} \cdot r \sin \phi = \eta_\theta(t) \quad (\text{A13})$$

$$\dot{\phi} \cdot r = \eta_\phi(t) \quad (\text{A14})$$

$$\langle \vec{\eta}_i(t) \vec{\eta}_j(t') \rangle = 2D_r \delta_{ij} \delta(t - t') \quad (\text{A15})$$

$$\dot{\vec{X}} = \xi_{\vec{X}}(t) \quad (\text{A16})$$

$$\langle \vec{\xi}_i(t) \vec{\xi}_j(t') \rangle = 2D_{\vec{X}} \delta_{ij} \delta(t - t') \quad (\text{A17})$$

Where we have introduced effective parameters related to the original ones:

$$\varepsilon_r \equiv m / \gamma_r, \quad \gamma_r \equiv \gamma / 2 \Rightarrow D_r \equiv 2 \cdot D_{phys} = \frac{k_b T}{\gamma_r} \quad (\text{A18})$$

$$D_X \equiv \frac{1}{2} \cdot D_{phys} = \frac{k_b T_X}{\gamma} \Leftrightarrow T_X \equiv \frac{1}{2} \cdot T_{phys} \quad (\text{A19})$$

⁴ This precludes our polynomial and unequal LJ potentials

Unfortunately equations (A13) & (A14) depend on r and do not nicely decouple however equation (A12) is identical to (4). This means that the 1-D motion of a single particle in a global potential is equivalent to the change in radial separation between two equal mass particles with an equivalent interaction potential. The centre of the mass of the two particles is described by a simple diffusion equation i.e. the centre of mass goes on a random walk in the dimension of the problem.

Appendix B: Stochastic action from Euclidean Schroedinger equation

We can rewrite the vector version of the Langevin equation (4) in terms of a probability distribution:

$$P(\vec{x}, t) = \langle \delta(\vec{x} - \vec{x}_\eta) \rangle \quad (\text{B1})$$

Where x_η is the solution to the vector Langevin equation for a given noise function η . This gives us the simple partial differential equations known as the Fokker-Planck (F-P) equation:

$$\frac{\partial P(\vec{x}, t)}{\partial t} = \varepsilon \nabla \cdot (P(\vec{x}, t) \nabla V) + D \nabla^2 P(\vec{x}, t) \quad (\text{B2})$$

If we rescale the probability like so:

$$P(\vec{x}, t) = e^{-\varepsilon V/2D} \tilde{P}(\vec{x}, t) \quad (\text{B3})$$

The F-P equation takes the following form:

$$D \frac{\partial \tilde{P}(\vec{x}, t)}{\partial t} = D^2 \nabla^2 \tilde{P}(\vec{x}, t) + \left(\frac{\varepsilon D}{2} \nabla^2 V - \frac{\varepsilon^2}{4} (\nabla V)^2 \right) \tilde{P}(\vec{x}, t) \quad (\text{B4})$$

This is simply the Euclidean Schroedinger equation as seen by making the following identifications: ⁵

$$M \equiv 1/2 \quad (\text{B5})$$

$$\hbar \equiv D \quad (\text{B6})$$

$$U(\vec{x}) \equiv \frac{\varepsilon^2}{4} (\nabla V(\vec{x}))^2 - \frac{\varepsilon D}{2} \nabla^2 V(\vec{x}) \quad (\text{B7})$$

Where $U(\vec{x})$ is the Schroedinger potential. If we have a Schroedinger equation then we can write this as a path integral. For our F-P equation we can then express the propagator as:

$$\begin{aligned} \langle \vec{x}_f, t_f | \vec{x}_i, t_i \rangle &= \mathcal{N} \exp \left(\frac{\varepsilon}{2D} [V(\vec{x}_f) - V(\vec{x}_i)] \right) \\ &\times \int \mathcal{D}\vec{x}(\tau) \exp \left(-\frac{1}{D} \int d\tau \frac{1}{4} (\partial_\tau \vec{x})^2 + U(\vec{x}) \right) \end{aligned} \quad (\text{B8})$$

⁵ N.B. the identification (B5) does not restrict us in any way as the mass M refers to the mass of a particle in the Schroedinger equation and has no bearing on the mass m of the particle in Brownian motion

The exponential prefactor has come from the fact that we redefined our physical probability $P(\mathbf{x}, t)$ in equation (B3) and we must rescale back in order to get the physical probability.

Appendix C: The equilibrium flow equation

In equilibrium, all expectation values can be generated by the generating function

$$Z(J) = \int dx e^{-V(x)/\Upsilon + Jx} \quad (\text{C1})$$

in a manner directly analogous to that described in the text but with functional derivatives replaced by ordinary derivatives w.r.t. J . In a spirit identical to the renormalization group but in the simpler setting of one degree of freedom, we can define a modified generating functional [21]

$$Z_k(J) = \int dx e^{-V(x)/\Upsilon - \frac{1}{2} R(k)x^2 + Jx} \quad (\text{C2})$$

with an additional quadratic term controlled by an arbitrary function $R(k)$ of a parameter k , satisfying $\lim_{k \rightarrow 0} R(k) = 0$, giving back the original $Z(J)$. Correlation functions are generated by $W_k(J) = \ln Z_k(J)$

$$\chi_k \equiv \langle x \rangle_k = \frac{\partial W_k(J)}{\partial J}, \quad \langle x^2 \rangle_k - \chi_k^2 = \frac{\partial^2 W_k(J)}{\partial J^2} \quad (\text{C3})$$

e.t.c. In the limit $k = 0$ and after setting $J = 0$ the usual predictions of the equilibrium Boltzmann distribution are recovered.

The source J has been considered as an external, independent variable controlling expectation values such as χ and higher correlators. One could also consider χ as the independent variable, solving $\chi = \partial W / \partial J$ for $J(\chi)$ and defining the effective potential $U(\chi)$ via a Legendre transform

$$\Gamma_k(\chi) + W_k(J) = J\chi - \frac{1}{2} R(k)\chi^2 \quad (\text{C4})$$

with

$$\Gamma(\chi) \equiv U(\chi)/\Upsilon \quad (\text{C5})$$

Note that

$$\frac{\partial \Gamma_k}{\partial \chi} = J_k - R(k)\chi \quad (\text{C6})$$

implying that the minimum of the effective potential defines the equilibrium expectation value of x (at $J = 0$ and $k = 0$).

The dependence of the generating function $W_k(J)$ on k can be easily obtained as

$$\partial_k W_k(J) = -\frac{1}{2} \partial_k R \left[\frac{\partial^2 W_k(J)}{\partial J^2} + \left(\frac{\partial W_k(J)}{\partial J} \right)^2 \right] \quad (\text{C7})$$

which is an ‘‘RG equation’’ for $W_k(J)$. We can also obtain an equation determining how $\Gamma_k(\chi)$ runs with k . Reciprocally, taking χ as the independent variable, J becomes a function of χ and k . Taking a k derivative of (C6) at fixed χ we obtain

$$\partial_k \Gamma_k(\chi) = \frac{1}{2} \partial_k R \frac{\partial^2 W_k}{\partial J^2} \quad (\text{C8})$$

To express the rhs in terms of $\Gamma_k(\chi)$, consider the first relation of (C3). Taking a χ derivative we find

$$\left(\frac{\partial^2 \Gamma_k}{\partial \chi^2} + R \right) \frac{\partial^2 W_k}{\partial J^2} = 1 \quad (\text{C9})$$

Hence, the ‘‘RG flow’’ of Γ is determined by

$$\partial_k \Gamma_k(\chi) = \frac{1}{2} \partial_k R \left(\frac{\partial^2 \Gamma}{\partial \chi^2} + R \right)^{-1} \quad (\text{C10})$$

Note also that, at $k \rightarrow 0$

$$\langle x^2 \rangle - \chi^2 = \frac{\Upsilon}{\partial_\chi^2 U(\chi_{eq})} \quad (\text{C11})$$

and hence the variance at equilibrium is determined by the curvature of the effective potential around its minimum.

All the above manipulations can be straightforwardly generalized to many or even infinite degrees of freedom and continuum actions, leading to the Wetterich equation (1), which is directly equivalent to (C10), and the relations of section (IV A). Note also that the equilibrium effective potential obeys the LPA flow equation exactly if we choose $R(k) = k$.

-
- [1] N. G. Van Kampen, *Stochastic Processes in Physics and Chemistry* (Elsevier, 2007).
- [2] C. Gardiner, *Stochastic methods*, Vol. 4 (2009).
- [3] A. A. Starobinsky and J. Yokoyama, Equilibrium state of a self-interacting scalar field in the de Sitter background, *Physical Review D* **50**, 6357 (1994).
- [4] K. G. Wilson, The renormalization group and critical phenomena, *Reviews of Modern Physics* **55**, 583 (1983).
- [5] M. E. Peskin and D. V. Schroeder, *An Introduction to quantum field theory* (Addison-Wesley, Reading, USA, 1995).
- [6] P. M. Chaikin and T. C. Lubensky, *Principles of Condensed Matter Physics* (Cambridge University Press, 1995).
- [7] C. Wetterich, Exact evolution equation for the effective potential, *Physics Letters B* **301**, 90 (1993), arXiv:arXiv:1710.05815v1.
- [8] T. R. Morris, The exact Renormalization group and approximate solutions, *International Journal of Modern Physics A* **09**, 2411 (1994).
- [9] J. Berges, N. Tetradis, and C. Wetterich, Non-perturbative renormalization flow in quantum field theory and statistical physics, *Physics Report* **363**, 223 (2002), arXiv:0005122 [hep-ph].
- [10] H. Gies, Introduction to the functional RG and applications to gauge theories, *Lecture Notes in Physics* **852**, 287 (2012), arXiv:0611146 [hep-ph].
- [11] B. Delamotte, An introduction to the nonperturbative renormalization group, *Lecture Notes in Physics* **852**, 49 (2012), arXiv:0702365 [cond-mat].
- [12] J. Niel and J. Zinn-Justin, Finite size effects in critical dynamics, *Nuclear Physics B* **280**, 355 (1987).
- [13] J. Zinn-Justin, *Quantum Field Theory and Critical Phenomena*, International series of monographs on physics (Clarendon Press, 2002).
- [14] C. Duclut and B. Delamotte, Frequency regulators for the nonperturbative renormalization group: A general study and the model A as a benchmark, *Physical Review E* **95**, 012107 (2017), arXiv:1611.07301v3.
- [15] T. Prokopec and G. Rigopoulos, Functional renormalization group for stochastic inflation, *Journal of Cosmology and Astroparticle Physics* **2018** (8), arXiv:1710.07333.
- [16] G. Moreau and J. Serreau, Unequal time correlators of stochastic scalar fields in de Sitter space, *Physical Review D* **101**, 1 (2020), arXiv:1912.05358.
- [17] G. Moreau, *Nonperturbative dynamics of quantum fields in de Sitter spacetime*, Ph.D. thesis, APC Paris (2020).
- [18] F. Synatschke, G. Bergner, H. Gies, and A. Wipf, Flow equation for supersymmetric quantum mechanics, *Journal of High Energy Physics* **2009**, 028 (2009), arXiv:0809.4396.
- [19] A. W. Lau and T. C. Lubensky, State-dependent diffusion: Thermodynamic consistency and its path integral formulation, *Physical Review E - Statistical, Nonlinear, and Soft Matter Physics* **76**, 10.1103/PhysRevE.76.011123 (2007), arXiv:0707.2234.
- [20] L. Canet, H. Chaté, and B. Delamotte, General framework of the non-perturbative renormalization group for non-equilibrium steady states, *Journal of Physics A: Mathematical and Theoretical* **44**, 495001 (2011), arXiv:1106.4129.
- [21] M. Guilleux and J. Serreau, Quantum scalar fields in de Sitter space from the nonperturbative renormalization group, *Physical Review D* **92**, 084010 (2015), arXiv:1506.06183.
- [22] M. Guilleux and J. Serreau, Nonperturbative renormalization group for scalar fields in de Sitter space: Beyond the local potential approximation, *Physical Review D* **95**, 045003 (2017), arXiv:1611.08106.